

Layerwise Monitoring of Polymer Laser Sintering Using Thermal Imaging

Mostafa Abdelrahman* and Thomas L. Starr**

*Rapid Prototyping Center, **Chemical Engineering Department,
J.B. Speed School of Engineering, University of Louisville, Louisville, KY 40292

REVIEWED

Abstract

Polymer Laser Sintering (LS) is used increasingly for manufacture of end-use parts. Improved methods of monitoring the process are needed to certify the quality of these parts. This paper describes the use of high resolution infrared thermal imaging to monitor the temperature of individual layers before, during and after laser scanning. The time-temperature history of each point in a layer depends on process parameters and part geometry. This history also controls the sintering and crystallization process for a single volume element of the part and its mechanical properties. Proposed new process control schemes may use this monitoring data to ensure that all volume elements achieve full density. The proposed framework includes creating a 3D template of the input model. This template simulates the part fabrication in the SLS machine. Registration of this template to the monitor data creates a 3D quality certificate for the part.

Introduction

Laser sintering was first introduced mainly to create prototypes. However, its use has expanded to additive manufacturing (AM) of metal and polymer end-use parts [1]. Polymer laser sintering is an additive manufacturing method that converts layers of polymer powder into a dense 3D structure by selectively heating areas with a scanning laser. While this technology was developed more than 30 years ago all commercial machines operate with open loop control and limited monitoring of the process. Despite this limitation the process has seen increased use for manufacture of end-use products and for processing new, higher temperature polymers. Improved process monitoring and control is needed to fully realize the potential of this process.

Previous investigators used optical sensors for laser process monitoring [2, 3, 4, 5]. Chivel and Smurov [6] and others in [7] proposed to use a combination of digital CCD camera and a single spot sensor-pyrometer for process monitoring. Diller et.al. [8] proposed to use thermal imaging for monitoring laser sintering process. They propose to analyze the temperature distribution on the powder bed surface. Thermal imaging systems have been integrated into the laser sintering systems to monitor the thermal history, correlate the outcomes and plan an optimized approach for part manufacture in [9, 10, 11]. Also the work by Schwerdtfeger et.al. [12] has been successful in identifying part defects with the use of thermal imagery.

None of these methods take full advantage of the layerwise, model-driven nature of this process. A new monitoring method is presented in this paper. This method uses the model geometry and layer information to index monitor data to the 3D geometry of the manufactured part. This method can be used with any layerwise AM process and any type of process monitor data. This paper uses infrared thermal imaging of the polymer LS process to demonstrate the method.

Approach

The layerwise quality monitoring method indexes monitor data to the part geometry using the part solid model and its build orientation and layer thickness. The method includes:

1. Slicing of the part solid model into layers of a specified thickness. This layer information is:
 - Sent to the AM machine and used for fabrication of the physical 3D part.
 - Digitized and stacked to form a **template** for the monitor data.
2. Monitoring of the fabrication process during manufacture of the part. Monitor data may include:
 - Slowly changing, continuous monitor data, e.g. built surface temperature or oxygen level, that are collected at regular time intervals and stored with a time-stamp.
 - **Layerwise monitor data**, e.g. IR (as in this paper) or visible-range camera images that are collected as 2D images of a particular layer of the part during its manufacture.
 - Process log, including for example, the start and finish time for each layer, the sequence of formation for each volume element within the layer (i.e. scan pattern) and process control parameters.
3. Indexing of monitor data to the template.
 - For continuous monitor data the value stored in the template is based on a layer index from the machine or a time-stamp relating the monitor value to a particular layer in the template. The monitor value is the same for every point in the layer.
 - For layerwise monitor data the value stored in the template is based on the 2D location within the layer and the location of that layer in the template. For example, indexing of layerwise monitor data may involve transformation of a camera image to the layer coordinate system in order to determine the relationship between the pixel value and the 3D location in the template. Layerwise data may be either an instantaneous record of the layer fabrication process or a **combined record** that is composed of a series of instantaneous records taken during fabrication of a layer.
 - Indexing of monitor data may be performed in real-time during the fabrication process or after completion of the build using stored monitor data.

Template Creation

The template is created using the actual layer information that is input to the AM machine. For any 3D part the layers depend on build orientation and specified layer thickness. Both of these characteristics are set by the machine operator just prior to starting the build.

While other formats for layer geometry are available, the CLI format (Common Layer Interface [13]) is non-proprietary and can be generated during build setup to match the orientation and layer thickness that the operator chooses. The CLI file for a specific part and specific build describes the outline of each layer. The AM machine fills this outline by scanning a laser with a raster pattern that is generated within the AM machine. While the specific raster pattern for each layer may not be known, the distance between individual scan lines is specified. This dimension determines the characteristic dimension of the laser melting process and is used to specify the hatch dimension in the template.

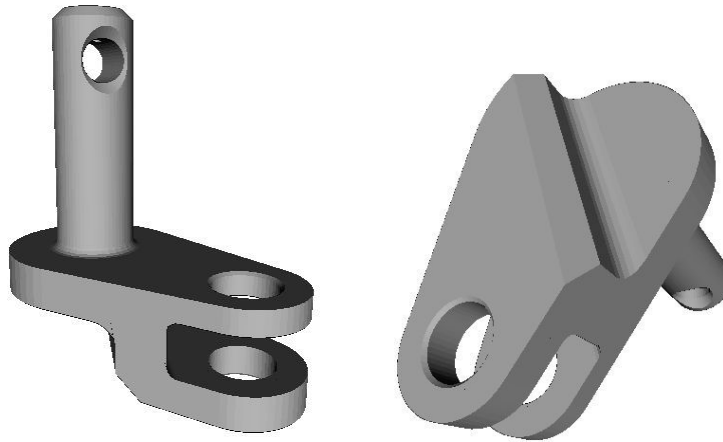


Figure 1, Rendering of STL file for part for AM in two different views. Build direction is vertical upwards in the left view.

Fig. 1 shows a 3D part with approximate dimensions $13.6 \times 7.5 \times 14.4$ mm. When built with 0.1016 mm (0.004 in) layer thickness in the orientation shown on the left, this part has 142 layers. The 12th and 38th layers have the geometry shown in Fig. 2. The CLI file specifies the layer geometry with coordinates of vertex points (to be connected by straight lines) and a direction. For a layer with a hole, such as this, two lines are defined with opposite directions. Hatching each layer in the CLI file, the binary layer images are stored in a single TIFF file. This 3D image file will be used to register process monitoring data. Fig. 3 is a rendering of the template volume. The template does not have a smooth surface since it matches the physical layer structure of the part used for the building process.

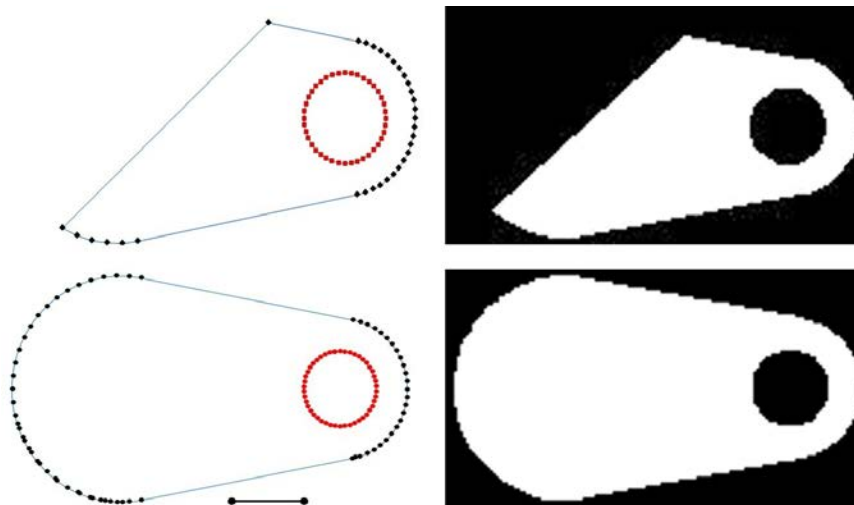


Figure 2. Left: CLI outline description of the layers number 12 and 38 for building the shape in Fig. 1. The scale bar is 5 mm. Right: Binary image (template) for layer with 0.1016 mm hatch dimension.

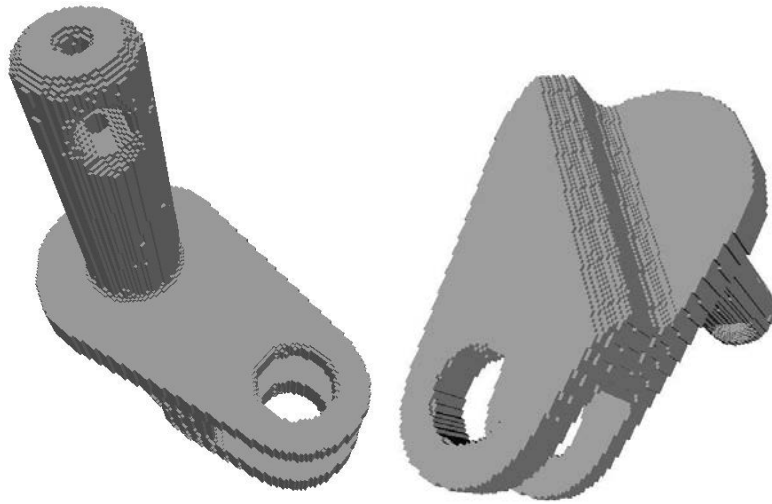


Figure 3. Volume rendering of template in two different views.

Data collection

Fig. 4 shows the experimental setup. The system consists of a polymer LS machine, thermal camera and a computer. The LS machine is the Sinterstation 2500+. The process is monitored by a FLIR SC7000 MWIR thermal camera. The camera operates in the 1.5 – 5.1 micron wavelength range with a full resolution of 640×512 pixels and a detector pitch of 15 micron. The frame rate of the camera can be 5 Hz to 100 Hz when using full window and up to 3.4 kHz with reduced window. The thermal sensitivity of the camera is 25 milliKelvins(mK). The thermal camera is mounted as shown in Fig. 5 to view the powder bed through a ZnSe window with transmittance equal to 70% in the camera's wavelength range. The camera is focused manually on



Figure 4. System setup consists of LS machine, thermal camera and a computer.

the region where the part will be built. For this experiment a 50 mm focal length lens is used and the frame rate set to 100 fps with window size of 336x216. The LS machine takes about 74 minutes to build this part. The recorded data is ~500,000 frames of video stored as 62 GB in FLIR's SAF file format. This data must be converted to actual temperatures and the frames parsed into individual layers.

Data Analysis

The raw intensity data is mapped to the real temperature values using a 1st-order mapping function. The real temperature values for two points, one point inside the part and another point outside the part, are recorded from the FLIR EXamineIR software. The emissivity is set to 0.90 inside the part and 1.00 outside the part in the software. The transmittance is set to 70% to compensate for the ZnSe window attenuation. The corresponding raw data for these points are extracted from the SAF file and used to determine a linear mapping from the raw data to the real temperature for each emissivity value. The recorded raw data for the entire build are then mapped to the actual temperatures (for emissivity = 1.00).

The frames are parsed into individual layers using the using the maximum temperature in each frame as a marker. Fig. 5 shows this marker for the first 12,000 frames, annotated to show the different parts of the LS process. For this build the minimum layer time was set to 30 seconds (3000 frames). Since the part is small the actual scan time for a layer is less than 1.5 seconds, i.e. the actual laser scan is recorded in just 150 frames. These are extracted for each layer for further processing.

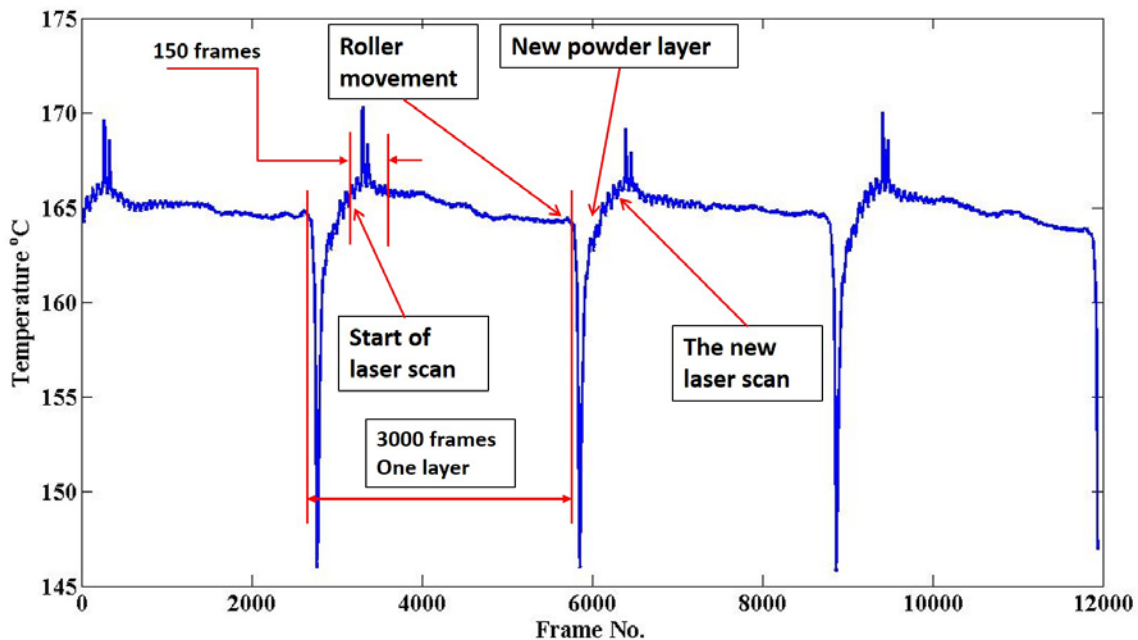


Figure 5. The maximum frame temperature for the first 12,000 frames accurately divides the video into parts. Each part records one layer build.

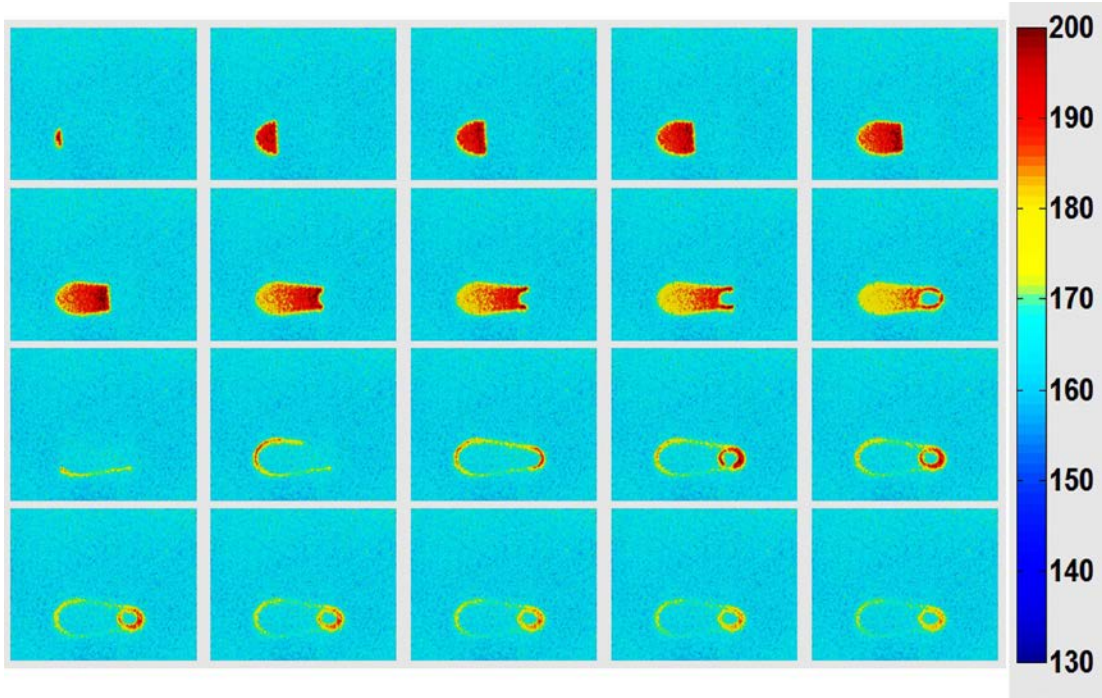


Figure 6. A sample of the video frames during the first layer scan. Upper two rows show scan of the interior of the part. The lower two rows show scan of the part outline.

Fig. 6 represents a sample of video frames during the first layer scan. The laser scanning process involves scanning the interior of the layer then scanning the outlines. For good densification every point of every layer of the part must be heated to a sufficiently high temperature. For each set of 150 frames the peak temperature value is detected for each point in the window area. These peak temperature values are assembled to form a single image for each layer. The second column of Fig. 8 shows images of maximum temperature during the scan for selected layers. These images will be used to create an indexed volume for defect detection.

Registration of Data to Template

The template layer (source) is registered to the corresponding peak temperature image (target) by estimating a projective transformation between the source template and the target image. The transformation is estimated between the edges of the template and the edges of the initially segmented image using fixed threshold. Given a source shape model \mathbf{M}_s that represents the template layer edges, and a target shape \mathbf{M}_t that represents the initially segmented image edges, a transformation \mathbf{A} that moves points from \mathbf{M}_s to \mathbf{M}_t is needed. The selected transformation has a set of parameters that will be estimated to minimize a certain energy function, similar techniques used before to estimate an affine transformation. Assume that the transformation is a 2D projective and hence it will have the following homogeneous format:

$$\mathbf{A} = \begin{pmatrix} a_1 & a_2 & a_3 \\ a_4 & a_5 & a_6 \\ a_7 & a_8 & a_9 \end{pmatrix} \quad (1)$$

Assume that $x_i \in \mathbf{M}_s, i = 1, 2, \dots, N_s$ and $y_i \in \mathbf{M}_t$ is the closest point to $\mathbf{A}x_i$ on the target shape where N_s is the number of points on the source surface. Note that both $x_i = \begin{pmatrix} x_{i1} \\ x_{i2} \\ 1 \end{pmatrix}$ and $y_i = \begin{pmatrix} y_{i1} \\ y_{i2} \\ 1 \end{pmatrix}$ points are put in the homogeneous vector notation of size 3×1 . Consider the Euclidean distance between the moved point and its closest position to be the dissimilarity measure as follows:

$$d_i = \|\mathbf{A}x_i - y_i\|. \quad (2)$$

And hence, the summation of squared differences can be written as the objective energy function:

$$E = E(a_1, a_2, \dots, a_9) = \sum_{i=1}^{N_s} \frac{1}{2} (\mathbf{A}x_i - y_i)^T (\mathbf{A}x_i - y_i) \quad (3)$$

Dividing by two to remove numbers from the derivative equations as follows. The transformation parameters $\{a_k\}$ are required to minimize the above functional. Taking the derivative of the energy with respect to a_k will result in:

$$\frac{\partial E}{\partial a_k} = \sum_{i=1}^{N_s} (\mathbf{A}x_i - y_i)^T (\mathbf{A}_{a_k} x_i) \quad (4)$$

where \mathbf{A}_{a_k} is the derivative of the transformation matrix \mathbf{A} with respect to the parameter a_k . So, any element $\mathbf{A}_{a_k}(m, n)$ in row m and column n of the derivative matrix can be written in the following format:

$$\mathbf{A}_{a_k}(m, n) = \begin{cases} 1 & \text{if } k == 3(m-1) + n \\ 0 & \text{otherwise} \end{cases} \quad (5)$$

Taking derivatives with respect to all the 9 parameters will result in a linear system of equations as shown below:

$$\Psi \Theta = \Lambda \quad (6)$$

where $\Theta = (a_1, a_2, \dots, a_8, a_9)^T$. The column vector Λ has 12 elements defined as follows:

$$\Lambda = \sum_{i=1}^{N_s} \begin{pmatrix} x_{i1}y_{i1} \\ x_{i2}y_{i1} \\ y_{i1} \\ x_{i1}y_{i2} \\ x_{i2}y_{i2} \\ y_{i2} \\ x_{i1} \\ x_{i2} \\ 1 \end{pmatrix} \quad (7)$$

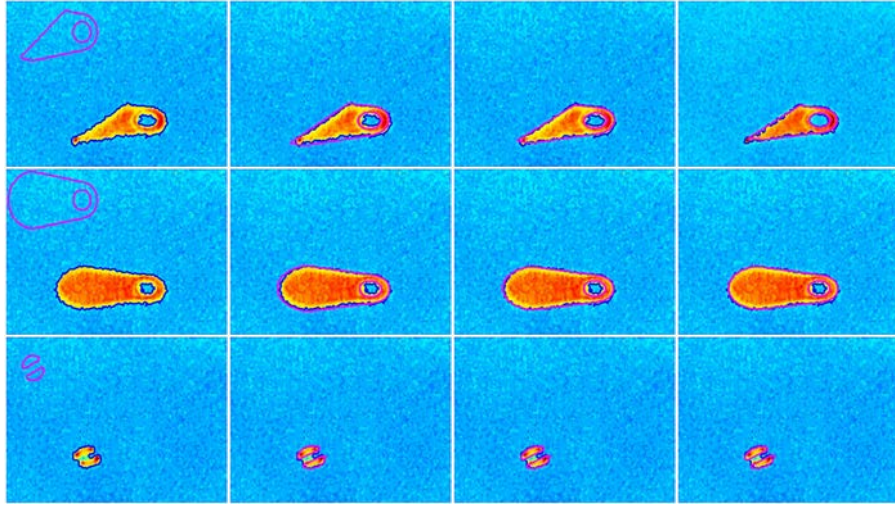


Figure 7. For three different layers, images from left to right are: initial position of template and target shapes, the registered template to target at the first iteration, at the third iteration and at the last iteration (about 10 iterations are needed). Template is in magenta and target is in blue.

The square matrix Ψ has 9×9 elements,

$$\Psi = \sum_{i=1}^{N_s} \begin{pmatrix} X_{ij} & 0 & 0 \\ 0 & X_{ij} & 0 \\ 0 & 0 & X_{ij} \end{pmatrix} \quad (8)$$

Where

$$X_{ij} = \begin{pmatrix} x_{i1}^2 & x_{i1}x_{i2} & x_{i1} \\ x_{i1}x_{i2} & x_{i2}^2 & x_{i2} \\ x_{i1} & x_{i2} & 1 \end{pmatrix} \quad (9)$$

Solving the above linear system will compute the parameters of the projective transformation that minimizes the distance between the two shape models. This process is repeated on the transformed shape until the change in the transformed points is not significant. Fig. 7 shows the registration process for three different layers. Fig. 8. shows the part segmentation results for eight different layers.

Once the part volume is segmented the temperatures within the part are recomputed taking into account the lower emissivity (0.90) of solid polymer as compared to the powder (1.00).

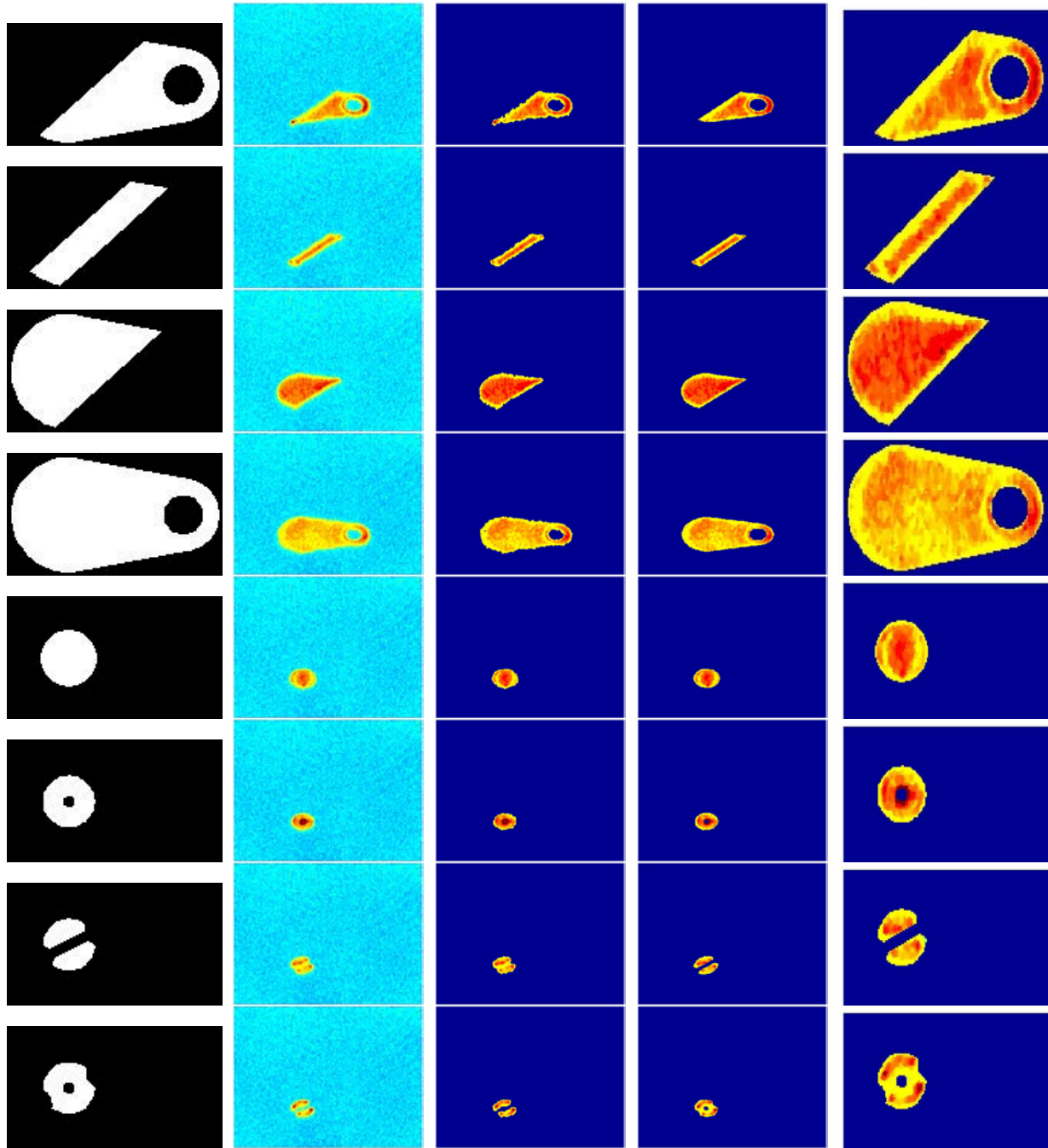


Figure 8. Images from left to right are: Template for different layers, maximum temperature during the scan, segmented images using threshold, segmented images using template-to-image registration, and segmented images mapped to template domain (Note that the color map is adjusted in segmented images in the three columns to the right for better visualization).

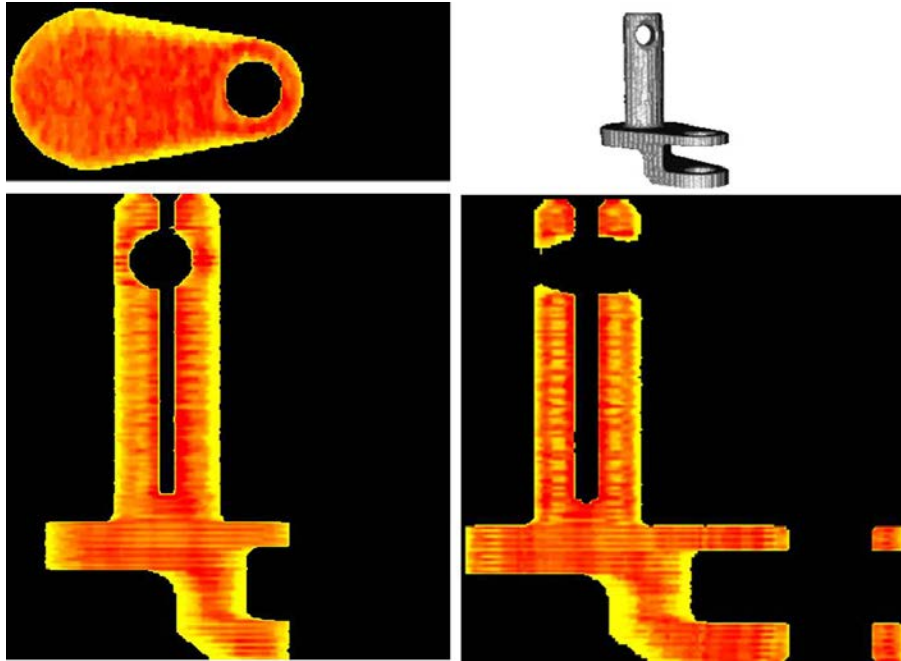


Figure 9: The 3D, axial, sagittal, and coronal views for the peak temperature volume after segmentation. The color represents the peak temperature at each point (red is higher than yellow). This figure shows the peak temperature variation from layer to layer and also inside the layer itself.

Analysis of Results

Fig. 9 shows the 3D, axial, sagittal, and coronal views for the peak temperature data after segmentation. This figure shows the differences in peak temperature value layer to layer and inside the layer itself. This figure confirms the need for improved control in order to get a uniform maximum temperature throughout the entire part. Defects can be created if the material within the scanned part does not reach the melting temperature or if material outside the part does. This part was built using PA 650 nylon 12 laser sintering material which has a melting point of $181\text{ }^{\circ}\text{C}$ [14]. Every point inside the part that does not reach a temperature higher $180\text{ }^{\circ}\text{C}$ could be a defect. Also, every point outside the part boundary that reached a temperature higher than $180\text{ }^{\circ}\text{C}$ could be a defect. Fig. 10 shows points that meet one of these criteria. There was no defect inside the part, i.e. every point within the part reached the melting temperature. However, some powder in the small vertical hole inside the part and near the part bottom was heated to the melting temperature. These defects, solid material attached to the part surface, was confirmed by visual inspection.

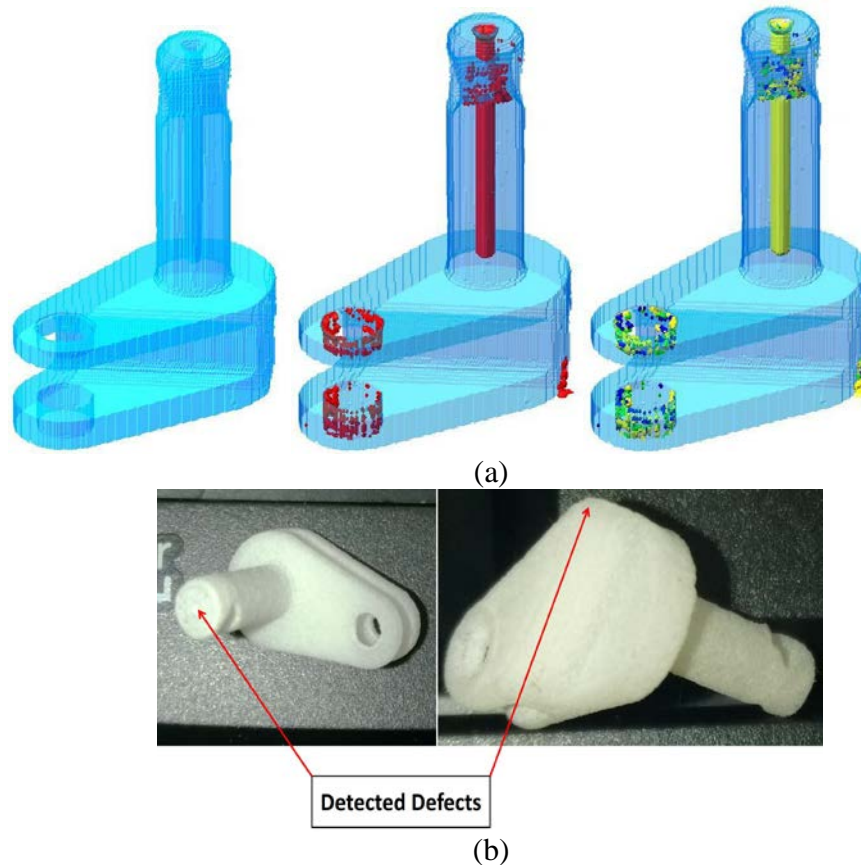


Figure 10. (a) Left: Part template, Middle: Defects on the boundaries of the part (points with temperature higher than $180\text{ }^{\circ}\text{C}$ are in red) , Right: Defects on the boundaries of the part (points with temperature higher than: 180 are in red, 181 are in green, 182 are in blue, and $183\text{ }^{\circ}\text{C}$ are in yellow). (b) Visual images for the part after build from two different views show the

Discussion

This paper addresses the problem of monitoring a layerwise additive manufacture process. A general approach to this problem is demonstrated for polymer laser sintering with process monitoring based on thermal imaging. Using the part model and information about how the part was orientated and sliced for the build allows indexing of voluminous monitoring data into an efficient 3D record of process conditions during creation of each volume element of the part. One important process condition is the peak temperature achieved during the scanning process. Results show that there is a relationship between this peak temperature value and presence or absence of defects in or near the part. Many other types of monitoring data can be used with this approach and correlations between these and the part geometry may provide further insight into the AM process and suggest control methods for maintaining part quality. The process record created in this approach can be considered a 3D quality certificate for the manufactured part.

References

- [1] Kumar, S., 2003. “Selective laser sintering: a qualitative and objective approach”. *JOM*, **55**(10), pp. 43–47.
- [2] Ignatiev, M., Smurov, I., and Flamant, G., 1994. “Real-time optical pyrometer in laser machining”. *Measurement Science and Technology*, **5**(5), p. 563.
- [3] Martinen, D., and Wohlfahrt, H., 1997. “Process monitoring in laser beam cutting on its way to industrial application”.
- [4] Smurov, I., 2007. “Laser process optical sensing and control”. In IV International WLT-Conference on Lasers in Manufacturing, pp. 537–546.
- [5] Doubenskaia, M., Pavlov, M., and Chivel, Y., 2010. “Optical system for on-line monitoring and temperature control in selective laser melting technology”. *Key Engineering Materials*, **437**, pp. 458–461.
- [6] Chivel, Y., and Smurov, I., 2010. “On-line temperature monitoring in selective laser sintering/melting”. *Physics Procedia*, **5**, pp. 515–521.
- [7] Doubenskaia, M., Pavlov, M., Grigoriev, S., Tikhonova, E., and Smurov, I., 2012. “Comprehensive optical monitoring of selective laser melting”. *Journal of Laser Micro Nanoengineering* 7.3, pp. 236–243.
- [8] Diller, T.; Sreenivasan, R. B. J. B. D. L. J., 2010. “Thermal model of the build environment for polyamide powder selective laser sintering”. Proceedings of the 21st Annual International Solid Freeform Fabrication Symposium (SFF 2010), The University of Texas at Austin, pp. 539–548.
- [9] Wegner, A., and Witt, G., 2011. “Process monitoring in laser sintering using thermal imaging”. In Proceedings of the 22nd Annual International Solid Freeform Fabrication Symposium (SFF 2011), The University of Texas at Austin, pp. 405–414.
- [10] Rodriguez, E., Medina, F., Espalin, D., Terrazas, C., Muse, D., and Henry, C., 2012. “Integration of a thermal imaging feedback control system in electron beam melting”. Proceedings of the 23rd Annual International Solid Freeform Fabrication Symposium (SFF 2012), The University of Texas at Austin, pp. 945–961.
- [11] Karnati, S., Matta, N., Sparks, T., and Liou, F., 2013. “Vision-based process monitoring for laser metal deposition processes”. In Proceedings of the 24rd Annual International Solid Freeform Fabrication Symposium (SFF 2013), The University of Texas at Austin.
- [12] Schwerdtfeger, J., Singer, R. F., and Körner, C., 2012. “*In situ* flaw detection by ir-imaging during electron beam melting”. *Rapid Prototyping Journal*, **18**(4), pp. 259–263.
- [13] Common layer interface. http://www.forwiss.uni-passau.de/welisch/papers/cli_format.html.
- [14] Pa 650 Technical Data Sheet, Advanced Laser Materials LLC, Temple, TX

Acknowledgement: This work is supported by the National Institutes of Standards and Technology and by AmericaMakes, the National Additive Manufacturing Institute.